Catalysis Today 139 (2008) 82–87

Contents lists available at ScienceDirect

Catalysis Today

journal homepage: www.elsevier.com/locate/cattod

Effect of hydrothermal treatment temperature on the catalytic performance of single-crystalline $La_{0.5}Sr_{0.5}MnO_{3-\delta}$ microcubes for the combustion of toluene

Jiguang Deng [a], Yue Zhang [a], Hongxing Dai [a,*], Lei Zhang [a], Hong He [a], C.T. Au [b,**]

[a] Laboratory of Catalysis Chemistry and Nanoscience, Department of Chemistry and Chemical Engineering, College of Environmental and Energy Engineering, Beijing University of Technology, Beijing 100124, PR China
[b] Department of Chemistry, Hong Kong Baptist University, Kowloon Tong, Hong Kong, PR China

ARTICLE INFO

Article history:
Available online 11 September 2008

Keywords:
Single-crystalline perovskite-type oxide
Microcube
Toluene oxidation
Volatile organic compounds
Hydrothermal synthesis

ABSTRACT

Perovskite-type oxide $La_{0.5}Sr_{0.5}MnO_{3-\delta}$ catalysts were fabricated hydrothermally at 220, 240, 250 or 270 °C for 50 h (denoted as LSMO-220, LSMO-240, LSMO-250, and LSMO-270, respectively). We characterized the materials by a number of analytical techniques. It was found that the $La_{0.5}Sr_{0.5}MnO_{3-\delta}$ samples are single-crystalline cubic perovskite-type oxides in the form of microcubes. The as-fabricated samples displayed various surface and bulk compositions that can be related to the discrepancy in treatment temperature. The surface Mn/(La + Sr + Mn) ratio and the initial H_2 consumption rate at low-temperatures increase according to the sequence of LSMO-240 < LSMO-270 < LSMO-220 < LSMO-250. We observed that the surface Mn^{4+}/Mn^{3+} ratio and catalytic performance of the materials follow a similar order. The temperature for 100% toluene conversion over LSMO-250 was 280 °C. The excellent performance of the materials can be related to (i) Mn surface enrichment, (ii) high Mn^{4+}/Mn^{3+} ratio, (iii) oxygen nonstoichiometry, and (iv) single-crystalline structure of the catalysts.

© 2008 Elsevier B.V. All rights reserved.

1. Introduction

Volatile organic compounds (VOCs) emitted from industrial and transportation activities are hazardous. The oxidation of VOCs over solid catalysts is an effective way for VOCs removal. Perovskite-type oxides (ABO_3), especially those of the $La_{1-x}Sr_xMO_{3-\delta}$ (M = Co, Mn) categories, show good catalytic performance for the removal of hydrocarbons and oxygenates [1–3]. It is generally accepted that the catalytic activity of ABO_3 can be related to (i) surface area, (ii) defect nature and density, and (ii) B-site ion redox property of the material. These factors can be determined by the preparation method adopted. For example, after having investigated the hydrothermal synthesis of $La_{0.5}Sr_{0.5}MnO_3$ [4] and $La_{0.5}Ba_{0.5}MnO_3$ [5], Feng and coworkers pointed out that the fabrication conditions, such as hydrothermal temperature, hydrothermal time, nature of metal precursor, and base strength, exert an influence on the crystal phase composition, manganese ion oxidation state distribution, and defect structure.

In the past two decades, researchers have been working on the fabrication and catalytic applications of nano- and micro-crystallites. The materials with distinct morphology have been proven to be superior to their irregular counterparts in catalytic performance [2,6–8]. The $La_{1-x}Sr_xMnO_{3-\delta}$ catalysts reported in the literature are mostly polycrystalline, and it is rare to come across single-crystalline $La_{1-x}Sr_xMnO_{3-\delta}$ in catalytic applications. Very recently, Teng et al. fabricated $La_{0.5}Sr_{0.5}MnO_{3-\delta}$ microcubes hydrothermally. They attributed the good catalytic activities of these single-crystallites in methane combustion to their unique structure and surface morphology [3].

Recently, we fabricated several series of ABO_3 by adopting various kinds of hydrothermal procedures, and observed that these materials exhibited excellent catalytic performance in the complete oxidation of VOCs. We herein report the influence of treatment temperature on the catalytic behaviors of the hydrothermally derived $La_{0.5}Sr_{0.5}MnO_{3-\delta}$ microcubes in toluene combustion.

2. Experimental

2.1. Catalyst fabrication

In a typical synthesis of $La_{0.5}Sr_{0.5}MnO_{3-\delta}$, 0.003 mol of $KMnO_4$, 0.007 mol of $MnCl_2{\cdot}4H_2O$, and stoichiometric amounts of lanthanum and strontium nitrates were dissolved in deionized (DI) water (total volume = 36 mL). Then 0.35 mol of KOH was added to the

* Corresponding author. Tel.: +86 10 6739 6588; fax: +86 10 6739 1983.
** Co-corresponding author.
E-mail addresses: hxdai@bjut.edu.cn (H. Dai), pctau@hkbu.edu.hk (C.T. Au).

0920-5861/$ – see front matter © 2008 Elsevier B.V. All rights reserved.
doi:10.1016/j.cattod.2008.08.010

mixture under ultrasonic stirring for 1 h. The solution was then transferred to a 50-mL Teflon-lined autoclave for hydrothermal treatment at 220, 240, 250 or 270 °C for 50 h. The obtained precursors were in turn washed with DI water, filtered, and dried at 120 °C overnight. The as-obtained catalysts are denoted as LSMO-220, LSMO-240, LSMO-250, and LSMO-270, respectively, hereinafter. For the purpose of comparison, we also prepared a polycrystalline $La_{0.5}Sr_{0.5}MnO_{3-\delta}$ catalyst (calcined at 950 °C for 4 h) by means of citric acid-complexing method [7]. All the chemicals (AR in purity) were purchased from Beijing Chemical Reagent Company and used without further purification.

2.2. Chemical analysis for Mn^{4+} content

The content of Mn^{4+} was determined by having a sample digested in known but excess amount of Mohr's salt ($Fe(NH_4)_2(SO_4)_2{\cdot}6H_2O$) standard solution that had been acidified with 1.00 mol L^{-1} H_2SO_4; the excess amount of Fe^{2+} was back titrated with 0.0167 mol L^{-1} $K_2Cr_2O_7$ in 3.00 mol L^{-1} HCl solution [9,10] using 0.5% sodium diphenylamine sulfonate solution as indicator. The error of such an experimental approach for the determination of Mn^{4+} content was estimated to be ±0.10%.

2.3. Catalyst characterization

The crystal phases of the as-fabricated samples were determined on an X-ray diffractometer (XRD, Bruker/AXS D8 Advance) operated at 40 kV and 200 mA using Cu Kα radiation (λ = 0.15406 nm) and nickel filter. The XRD patterns were recorded in the 2θ = 10–80° range. The specific surface areas of the samples were determined via N_2 adsorption at −196 °C on a Micromeritics ASAP 2020 apparatus with the samples outgassed at 250 °C for 2 h under vacuum prior to sample cooling and N_2 adsorption. The scanning electron microscopic (SEM) images of the samples were recorded on a JEOL JSM 6500F instrument, which was also equipped for energy-dispersive X-ray (EDX) analysis (operated at 30 kV). The transmission electron microscopic (TEM) images and selected area electron diffraction (SAED) patterns were obtained on a JEOL-2010 instrument (operated at 200 kV).

X-ray photoelectron spectroscopy (XPS, VG CLAM 4 MCD analyzer) was employed to determine the La 3d, Sr 2p, Mn 2p, O 1s, and C 1s binding energies (BEs) of surface entities of the as-synthesized samples using Mg Kα ($h\nu$ = 1253.6 eV) as excitation source. The instrumental resolution was 0.5 eV. Before XPS determination, the samples were calcined in O_2 (flow rate = 20 mL min^{-1}) at 500 °C for 1 h for the removal of surface carbonate and adsorbed water. The samples were then cooled to room temperature (RT), and under the protection of helium (GLOVE BAG, Instruments for Research and Industry, USA), mounted and transferred to the spectrometer. The samples were outgassed in the preparation chamber (10^{-5} Torr) for 0.5 h and introduced into the analysis chamber (3×10^{-9} Torr) for XPS recording. The C 1s peak at 284.6 eV was taken as a reference for BE calibration.

For the O_2 temperature-programmed desorption (O_2-TPD) studies, the sample (0.1–0.2 g) was placed in the middle of a quartz microreactor of 8-mm inner diameter (i.d.). The outlet gases were analyzed on-line by mass spectrometry (Hiden HPR20). Before each run, the sample was treated in O_2 (flow rate = 20 mL min^{-1}) at 500 °C for 1 h, followed by cooling in O_2 to RT and helium purging (flow rate = 40 mL min^{-1}) for 4 h. The purpose of helium purging was to remove gas-phase oxygen in the system. The sample was then heated (10 °C min^{-1}) from RT to 900 °C. The amount of O_2 desorbed from the catalyst was quantified by calibrating the peak area against that of a standard O_2 pulse (50.0 μL).

Hydrogen temperature-programmed reduction (H_2-TPR) was carried out in a quartz fixed-bed microreactor (i.d. = 6 mm) in the RT–900 °C range. Before each run, the sample (0.05–0.1 g) was treated in an oxygen flow (50 mL min^{-1}) at 500 °C for 1 h and then cooled down to RT under the same atmosphere. After being purged by a flow of N_2 (flow rate = 50 mL min^{-1}) for 30 min, the sample was reduced in a 5% H_2/Ar flow (50 mL min^{-1}) at a ramping rate of 10 °C min^{-1}. The effluent was monitored by a thermal conductivity detector. The thermal conductivity response was calibrated against the reduction of a known CuO powder sample (Aldrich, 99.995%).

2.4. Catalytic test

The catalytic activity was evaluated with the sample secured in a continuous flow fixed-bed quartz microreactor (i.d. = 8 mm) at atmospheric pressure. The catalyst (0.1–0.2 g, 40–60 mesh) was diluted with an equal amount of quartz sands (40–60 mesh). The reactant feed (flow rate = 33.3 mL min^{-1}) was 1000 ppm toluene + O_2 + N_2 (balance) with toluene/O_2 molar ratio being 1/400, and the space velocity was 20,000 h^{-1}. The outlet gases were analyzed on-line by a gas chromatograph (Shimadzu GC-2010) equipped with a flame ionization detector and a thermal conductivity detector, using a Chromosorb 101 column for toluene and a Carboxen 1000 column for permanent gas separation.

3. Results and discussion

3.1. Crystal structures, surface areas, and morphologies of catalysts

The crystal structures, compositions, oxygen nonstoichiometry, and surface areas of the $La_{0.5}Sr_{0.5}MnO_{3-\delta}$ catalysts are summarized in Table 1 and their XRD patterns are shown in Fig. 1. According to the XRD patterns, one can realize that the positions and relative intensities of the main diffraction peaks of $La_{0.5}Sr_{0.5}MnO_{3-\delta}$ resemble those of cubic $LaMnO_3$ (JCPDS PDF# 75-0440), indicating that the catalysts fabricated in the present work are of cubic perovskite-type structure. The XRD results demonstrate that cubic perovskite $La_{0.5}Sr_{0.5}MnO_{3-\delta}$ could be formed directly via hydrothermal treatment at 220 °C for 50 h without any need of high-temperature calcination. It is also observed that the BET surface areas of the four perovskite samples are less than 2 m^2 g^{-1}, in consistent with the microsizes of the particles as observed in SEM and TEM images illustrated below.

Fig. 2 shows the representative SEM and TEM images as well as SAED patterns of the LSMO-250 sample (images of the other three catalysts are not shown here). We find that the catalyst was composed of aggregates of intertwined microcubes with an

Table 1
Physical properties of the $La_{0.5}Sr_{0.5}MnO_{3-\delta}$ catalysts

Catalyst	Crystal phase	Mn^{4+}/Mn^{3+} (Bulk)	δ	Surface area (m^2 g^{-1})
LSMO-220	Perovskite + $La(OH)_3$ (trace)	0.86	0.0185	1.8
LSMO-240	Perovskite + $La(OH)_3$ (trace)	0.90	0.0125	1.8
LSMO-250	Perovskite + $La(OH)_3$ (trace)	1.02	−0.0025	1.8
LSMO-270	Perovskite + $La(OH)_3$ (trace)	0.86	0.0195	1.5

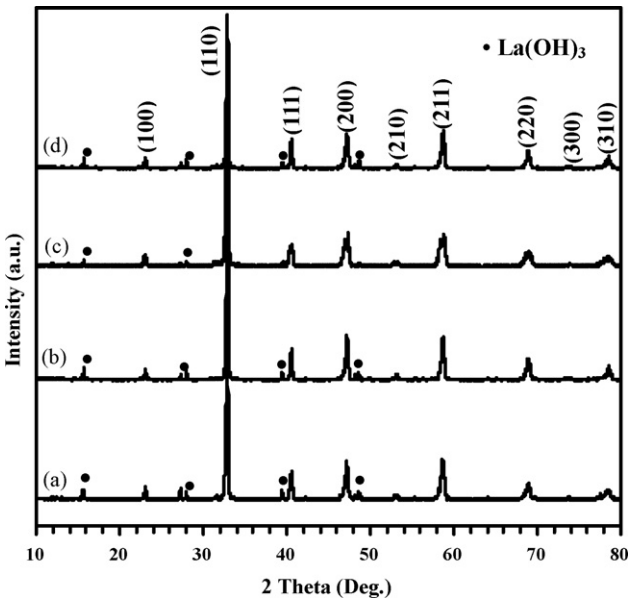

Fig. 1. XRD patterns of (a) LSMO-220, (b) LSMO-240, (c) LSMO-250, and (d) LSMO-270.

average size of 5–20 μm. In addition, we observe some "rod-shaped" entities (not shown here) with the diameter and length of 50–800 nm and 0.3–4.2 μm, respectively. The results of EDX analysis reveal that (i) the La:Sr:Mn atomic ratio of the microcubes was 1.00:0.98:2.02, similar to the nominal La:Sr:Mn atomic ratio (0.5:0.5:1.0); and (ii) the "rod-like" entities were mainly composed of La ions with a minute amount of Mn and Sr ions, showing a La:Sr:Mn atomic ratio of 23.1:1:1.8. It is apparent that the microcubes are made up of $La_{0.5}Sr_{0.5}MnO_{3-\delta}$ while the microrods are composed of $La(OH)_3$, in good agreement with the XRD results. The SAED pattern revealed that the microcubes are single-crystalline.

3.2. Mn^{4+} content and structural defects of catalysts

Table 1 summarizes the physical properties of the as-fabricated catalysts. The results of Mn oxidation state measurements show that the bulk Mn^{4+}/Mn^{3+} molar ratio was 0.86 for LSMO-220, 0.90 for LSMO-240, 1.02 for LSMO-250, and 0.86 for LSMO-270; on the basis of electroneutrality principle, the oxygen nonstoichiometry (δ) was estimated to be 0.0185, 0.0125, −0.0025, and 0.0195, respectively. It indicates that the LSMO-220, LSMO-240, and LSMO-270 catalysts exhibited reductive nonstoichiometry whereas the LSMO-250 catalyst displayed oxidative nonstoichiometry [11,12].

The results of XPS investigation (Fig. 3) reveal that there were two O 1s signals at BE = 529.2 and 531.7 eV corresponding to surface lattice and adsorbed oxygen species [13,14], with the LSMO-250 catalyst showing the highest amount of oxygen adspecies. The detection of Mn 2p signals at BE = 641.5 and 643.3 eV and at BE = 652.8 and 654.5 eV indicates the presence of Mn^{3+} and Mn^{4+} ions, respectively [15,16]. According to the surface compositions calculated according to the XPS results (Table 2), there is Mn enrichment on the surfaces, in concord with the results of other researchers [16,17]. From Table 2, one can find that the surface Mn/(La + Sr + Mn) ratios decreased in the order of LSMO-250 > LSMO-220 > LSMO-270 > LSMO-240. It is apparent that the surface Mn^{4+}/Mn^{3+} ratio was higher than the bulk Mn^{4+}/Mn^{3+} ratio.

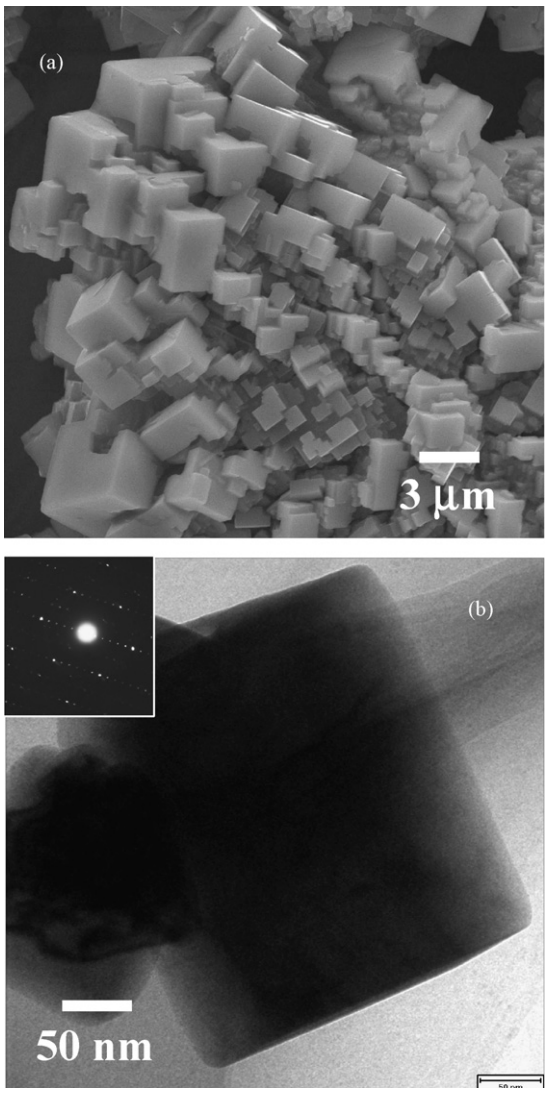

Fig. 2. SEM (a) and TEM (b) images as well as SAED pattern (inset) of LSMO-250.

3.3. Oxygen species and reducibility of catalysts

Shown in Fig. 4 are the O_2-TPD profiles of the $La_{0.5}Sr_{0.5}MnO_{3-\delta}$ samples. There was a weak desorption peak in the 250–500 °C

Table 2
XPS-derived surface molar compositions of the $La_{0.5}Sr_{0.5}MnO_{3-\delta}$ catalysts

Catalyst	La/Mn	Sr/Mn	La/Sr	Mn/(La + Sr + Mn)	$O_{ads}/O^{2-}{}_{latt}$	Mn^{4+}/Mn^{3+}
LSMO-220	0.40 (0.50)[a]	0.04 (0.50)	10.9 (1.0)	0.70 (0.50)	1.88	1.33
LSMO-240	0.78 (0.50)	0.17 (0.50)	4.65 (1.0)	0.51 (0.50)	1.88	1.23
LSMO-250	0.11 (0.50)	0.15 (0.50)	0.71 (1.0)	0.79 (0.50)	2.06	1.50
LSMO-270	0.81 (0.50)	0.09 (0.50)	8.94 (1.0)	0.53 (0.50)	1.70	1.40

[a] The data in parentheses were calculated according to the nominal compositions of $La_{0.5}Sr_{0.5}MnO_3$.

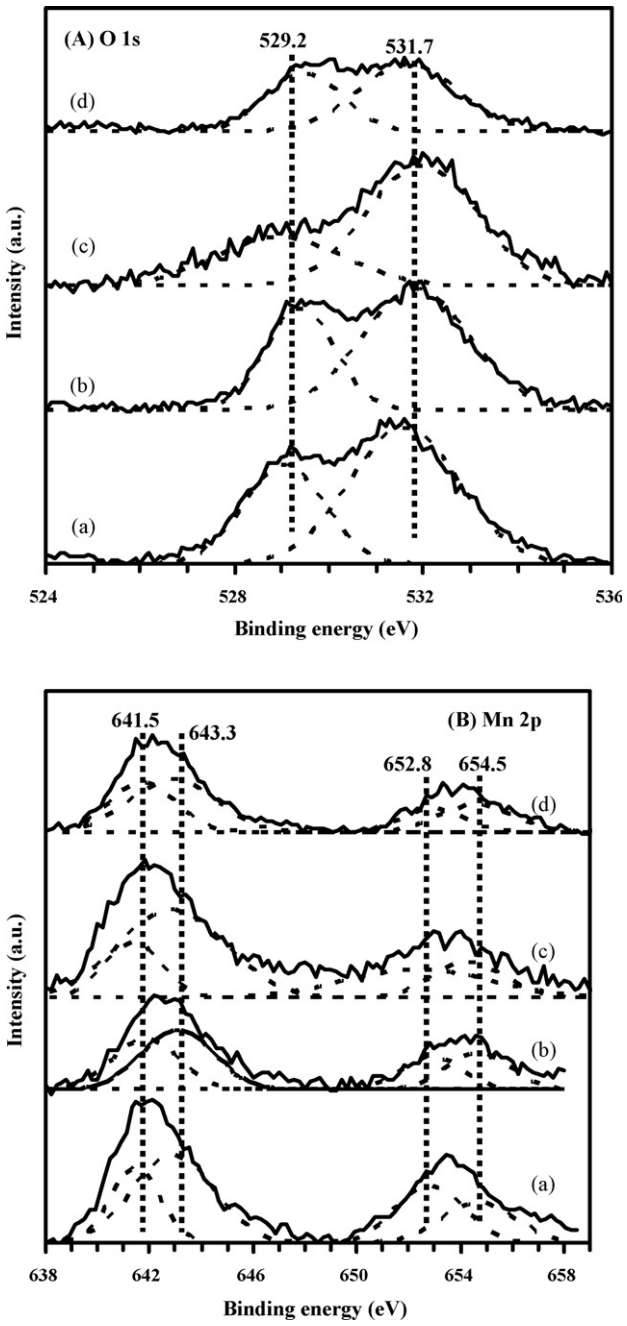

Fig. 3. (A) O 1s and (B) Mn 2p XPS spectra of (a) LSMO-220, (b) LSMO-240, (c) LSMO-250, and (d) LSMO-270.

range, the corresponding amount of oxygen desorption was estimated to be 2.4, 43.7, and 2.8 μmol g_{cat}^{-1} for the LSMO-220, LSMO-250 and LSMO-270 samples, respectively. There was a strong peak located in the 500–800 °C range, and another peak that started from ca. 800 °C. The amount of oxygen desorption in the 500–800 °C range was 168.9, 104.6, 105.3 and 113.7 μmol g_{cat}^{-1} for the LSMO-220, LSMO-240, LSMO-250, and LSMO-270 sample, respectively. According to Seiyama [18], the peaks below 500 °C can be attributed to the desorption of oxygen species adsorbed at surface vacancies, while the ones above 500 °C to the desorption of surface lattice oxygen due to the partial reduction of Mn-based perovskites. Based on the amount of oxygen desorption in the 250–500 °C range, we deduce that the surface density of oxygen vacancies of these catalysts decreased in the order of LSMO-250

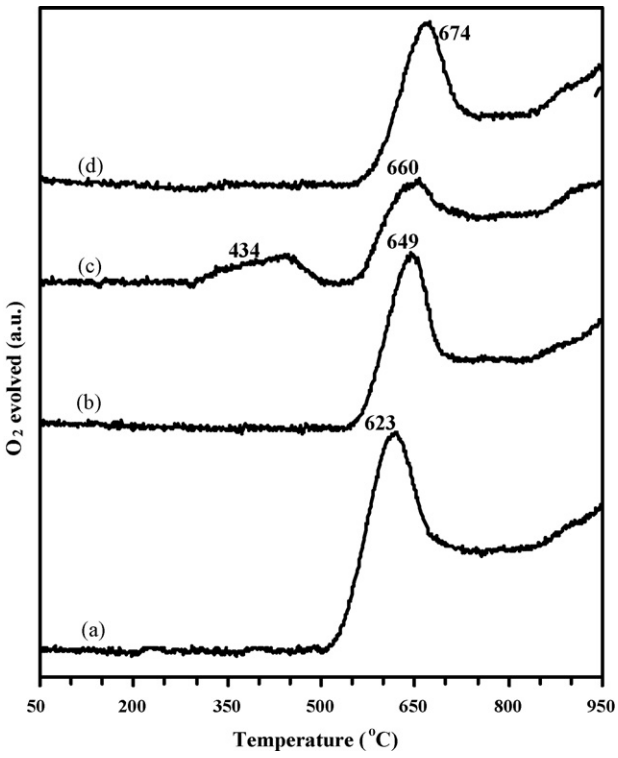

Fig. 4. O_2-TPD profiles of (a) LSMO-220, (b) LSMO-240, (c) LSMO-250, and (d) LSMO-270.

LSMO-220 ≈ LSMO-270 > LSMO-240. Fig. 5 shows the H_2-TPR profiles of the $La_{0.5}Sr_{0.5}MnO_{3-\delta}$ samples. There were two peaks for each sample (Fig. 5A). The first in the 200–600 °C range corresponded to a H_2 consumption of 2.32, 2.15, 2.43 and 2.29 mmol g_{cat}^{-1}, whereas that in the 650–820 °C range corresponded to 1.06, 1.02, 0.95 and 1.05 mmol g_{cat}^{-1} for the LSMO-220, LSMO-240, LSMO-250, and LSMO-270 sample, respectively. For better understanding on the reducibility of the four samples, we obtained the initial H_2 consumption rate in the temperature range of 250–295 °C (Fig. 5B). It is apparent that the initial consumption rate of the catalysts decreased in the order of LSMO-250 > LSMO-220 > LSMO-270 > LSMO-240. As illustrated in the next section, the catalytic performance of the single-crystalline ABO_3 followed a similar order.

3.4. Catalytic performance

Under the conditions of toluene concentration = 1000 ppm, toluene/O_2 molar ratio = 1/400, and space velocity = 20,000 h^{-1}, the toluene conversion increased with a rise in reaction temperature. The catalytic activity decreased in the sequence of LSMO-250 > LSMO-220 > LSMO-270 > LSMO-240 (Fig. 6). The light-off temperature $T_{50\%}$ (toluene conversion = 50%) and the temperature for complete combustion $T_{100\%}$ (toluene conversion = 100%) are ca. 261 and 310 °C over LSMO-220, 280 and 350 °C over LSMO-240, 252 and 280 °C over LSMO-250, and 270 and 330 °C over LSMO-270, respectively. The LSMO-250 catalyst outperformed the $LaMnO_3$ and $La_{0.8}Sr_{0.2}MnO_3$ catalysts over which the $T_{100\%}$ was found to be above 340 °C even at a low space velocity of 184 h^{-1} [19]. Under similar conditions, the polycrystalline $La_{0.5}Sr_{0.5}MnO_{3-\delta}$ (surface area = 5.3 m^2 g^{-1}) sample exhibited the $T_{50\%}$ and $T_{100\%}$ equal to 296 and 368 °C, respectively. It is clear that the high-temperature derived polycrystalline catalyst was inferior to its hydrothermally derived

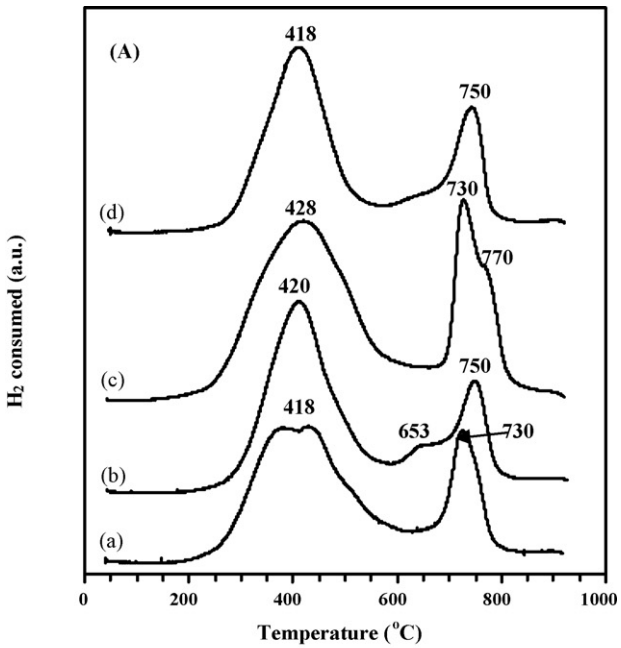

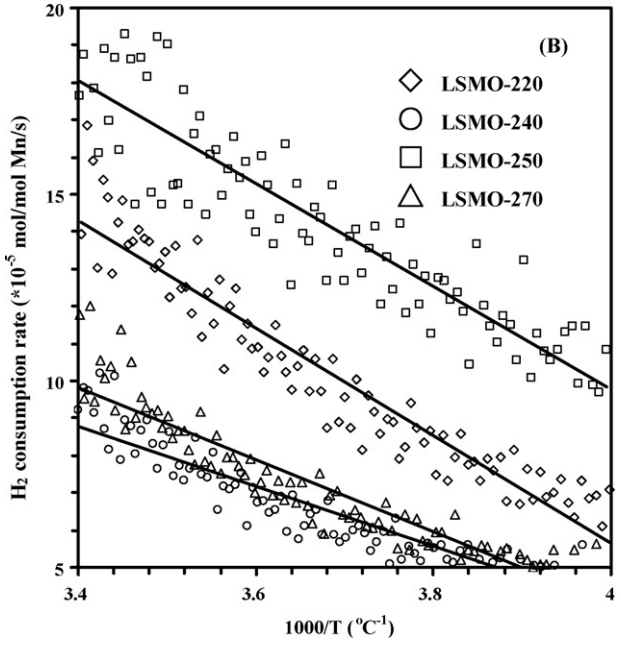

Fig. 5. (A) H_2-TPR profiles and (B) initial hydrogen consumption rate of (a) LSMO-220, (b) LSMO-240, (c) LSMO-250, and (d) LSMO-270.

single-crystalline counterparts. The discrepancy in activity might be related to the difference in oxygen nonstoichiometry and redox ability. It is worth pointing out that over the $La_{0.5}Sr_{0.5}MnO_{3-\delta}$ catalysts, toluene was completely oxidized to CO_2 and H_2O, as confirmed by the estimated carbon balance of 99.5%.

After having investigated the catalytic combustion of hydrocarbon over ABO_3, Seiyama and coworkers found that the catalytic activity of the ABO_3 materials is mainly dependent on the nature of the B-site component [18]. In other words, the B-site component is catalytically active in the reaction. According to the results of the present study, the order of the surface Mn/(La + Sr + Mn) ratio of the four catalysts agreed well with that of catalytic activity, implying that the surface Mn components provided active sites for the addressed reaction. According to the results of Machoki et al.

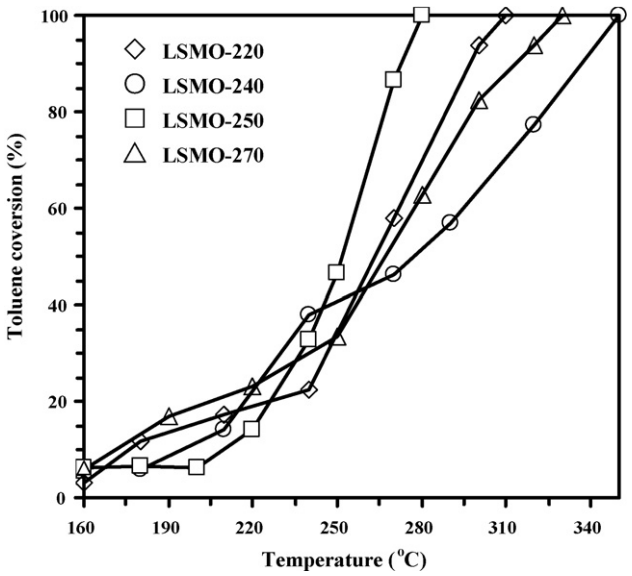

Fig. 6. Toluene conversion as a function of reaction temperature over $La_{0.5}Sr_{0.5}MnO_{3-\delta}$ under the conditions of toluene concentration = 1000 ppm, toluene/O_2 molar ratio = 1/400, and space velocity = 20,000 h^{-1}.

[17], Lisi et al. [20], and those of ours [2], we suggest that the catalytic activities of $La_{1-x}Sr_xMnO_{3-\delta}$ can be related to the nature of the redox processes: $Mn^{4+} \Leftrightarrow Mn^{3+}$. It has been shown in Section 3.2 that the bulk Mn^{4+}/Mn^{3+} ratio followed a sequence of LSMO-220 ≈ LSMO-270 < LSMO-240 < LSMO-250, whereas the surface Mn^{4+}/Mn^{3+} ratio increased in the order of LSMO-240 < LSMO-220 < LSMO-270 < LSMO-250 (Tables 1 and 2). Machoki et al. [17] demonstrated that the rate of methane oxidation over $LaMnO_3$ displayed a linear relationship with the surface Mn^{4+}/Mn^{3+} ratio. By comparing the catalytic performance of $La_{0.5}Sr_{0.5}MnO_{3-\delta}$ with the surface and bulk Mn^{4+}/Mn^{3+} ratios, one can see that the catalytic activity showed a better correlation with the surface Mn^{4+}/Mn^{3+} ratio. It means that the surface Mn^{4+}/Mn^{3+} ratio has a greater impact on catalytic activity.

Besides correlating surface Mn^{4+}/Mn^{3+} ratio with catalytic activity, the relationship between catalytic activity and bulk oxygen mobility (in terms of the reducibility of transition metal ions) has been discussed in context of hydrocarbon oxidation [21,22]. According to the results of catalytic evaluation and TPR experiments, we believe that the catalyst with a higher initial H_2 consumption rate in the 250–500 °C range should exhibit a higher activity for toluene combustion. It has been reported that the presence of oxygen vacancies could result in the promotion of oxygen diffusion and enhancement in the mobility of lattice O^{2-} [23,24]. As revealed in Fig. 4, the amount of oxygen vacancies on/in $La_{0.5}Sr_{0.5}MnO_{3-\delta}$ followed the order of LSMO-250 > LSMO-220 ≈ LSMO-270 > LSMO-240, which is similar to the sequence of catalytic performance.

4. Conclusion

In summary, single-crystalline cubic perovskite $La_{0.5}Sr_{0.5}MnO_{3-\delta}$ microcubes have been fabricated hydrothermally. The temperature for hydrothermal treatment has a remarkable effect on the nature of the $La_{0.5}Sr_{0.5}MnO_{3-\delta}$ catalysts. Among the four catalysts, the one fabricated hydrothermally at 250 °C showed the best activity for toluene oxidation. We conclude that the outstanding performance can be related to the factors, such as surface Mn enrichment, high Mn^{4+}/Mn^{3+} ratio, surface oxygen vacancies, and single-crystalline structure of the catalyst.

Acknowledgements

This work was supported by the NSF of Beijing Municipality (Key Class B project of grant No. KZ200610005004), the SRF for ROCS (State Education Ministry of China), and the PHR (IHLB) of Beijing Municipality. CTA thanks the RGC, Hong Kong Special Administration Region for financial support (Grant no. HKBU 200106).

References

[1] T. Seiyama, Catal. Rev. -Sci. Eng. 34 (1992) 281.
[2] J.R. Niu, J.G. Deng, W. Liu, L. Zhang, G.Z. Wang, H.X. Dai, H. He, X.H. Zi, Catal. Today 126 (2007) 420.
[3] F. Teng, W. Han, S. Liang, B. Gaugeu, R. Zong, Y. Zhu, J. Catal. 250 (2007) 1.
[4] D. Wang, R.B. Yu, S.H. Feng, W.J. Zheng, R.R. Xu, Y. Matsumura, M. Takano, Chem. Lett. 32 (2003) 74.
[5] D. Wang, R.B. Yu, S.H. Feng, W.J. Zheng, G.S. Pang, H. Zhao, Chem. J. Chin. Univ. 19 (1998) 165.
[6] L.G. Tejuca, J.L.G. Fierro, J.M.D. Tascon, Adv. Catal. 36 (1989) 237.
[7] S. Royer, F. Bérubé, S. Kaliaguine, Appl. Catal. A 282 (2005) 273.
[8] G. Sinquin, C. Petit, J.P. Hindermann, A. Kiennemann, Catal. Today 70 (2001) 183.
[9] R. Spinicci, M. Faticanti, P. Marini, S. De Rossi, P. Porta, J. Mol. Catal. A 197 (2003) 147.
[10] Y. Wu, T. Yu, B.S. Dou, C.X. Wang, X.F. Xie, Z.L. Yu, S.R. Fan, Z.R. Fan, L.C. Wang, J. Catal. 120 (1989) 120.
[11] M.A. Peña, J.L.G. Fierro, Chem. Rev. 101 (2001) 1981.
[12] L. Rørmark, K. Wiik, S. Stølen, T. Grande, J. Mater. Chem. 12 (2002) 1058.
[13] N. Yamazoe, Y. Teraoka, T. Seiyama, Chem. Lett. 10 (1981) 1767.
[14] J.L.G. Fierro, L.G. Tejuca, Appl. Surf. Sci. 27 (1987) 453.
[15] J.F. Moulder, W.F. Stickle, P.E. Sobol, K.D. Bomben, in: J. Chastain, R.C. King, Jr. (Eds.), Handbook of X-ray Photoelectron Spectroscopy, Physical Electronics, Inc., Eden Prairie, 1995, p. 78.
[16] S. Ponce, M.A. Peña, J.L.G. Fierro, Appl. Catal. B 24 (2000) 193.
[17] A. Machoki, T. Ioannides, B. Stasinska, W. Gac, G. Avgouropoulos, D. Delimaris, W. Grzegorczyk, S. Pasieczna, J. Catal. 227 (2004) 282.
[18] T. Seiyama, in: L.G. Tejuca, J.L.G. Fierro (Eds.), Properties and Applications of Perovskite-type Oxides, Marcel Dekker, New York, 1993, p. 215.
[19] S. Irusta, M.P. Pina, M. Menéndez, J. Santamaría, J. Catal. 179 (1998) 400.
[20] L. Lisi, G. Bagnasco, P. Ciambelli, S. De Rossi, P. Porta, G. Russo, M. Turco, J. Solid State Chem. 146 (1999) 176.
[21] S. Royer, D. Duprez, S. Kaliaguine, J. Catal. 234 (2005) 364.
[22] L. Borovskikh, G. Mazo, E. Kemnitz, Solid State Sci. 5 (2003) 409.
[23] H.X. Dai, H. He, P.H. Li, L.Z. Gao, C.T. Au, Catal. Today 90 (2004) 231.
[24] S. Royer, H. Alamdari, D. Duprez, S. Kaliaguine, Appl. Catal. B 58 (2005) 273.